Engineered muscle from micro-channeled PEG scaffold with magnetic Fe$_3$O$_4$ fixation towards accelerating esophageal muscle repair

Yang Luo [a,1], Yichen Chen [b,1], Zhaofeng Gu [c], Renhao Ni [a], Peipei Feng [d], Zeming Hu [a], Lei Song [b], Xiang Shen [c], Chenjie Gu [c], Jiajie Li [e], Tianyu Du [a], Lu Yang [e,*], Hua Zhang [a,f,**], Yabin Zhu [a,***]

[a] *Health Science Center, Ningbo University, Ningbo, 315211, China*
[b] *Ningbo Women and Children's Hospital, Ningbo, 315031, China*
[c] *Laboratory of Infrared Materials and Devices, Advanced Technology Research Institute, Ningbo University, Ningbo, 315211, China*
[d] *Ningbo Institute of Innovation for Combined Medicine and Engineering, Ningbo Medical Centre Lihuili Hospital, Ningbo, 315010, China*
[e] *The First Affiliated Hospital of Ningbo University, Ningbo, 315010, China*
[f] *State Key Laboratory of Fluid Power and Mechatronic Systems, Zhejiang University, Hangzhou, 310027, China*

ARTICLE INFO

ABSTRACT

Engineered scaffolds are used for repairing damaged esophagus to allow the precise alignment and movement of smooth muscle for peristalsis. However, most of these scaffolds focus solely on inducing cell alignment through directional apparatus, often overlooking the promotion of muscle tissue formation and causing reduced esophageal muscle repair effectiveness. To address this issue, we first introduced aligned nano-ferroferric oxide (Fe$_3$O$_4$) assemblies on a micropatterned poly(ethylene glycol) (PEG) hydrogel to form micro-/nano-stripes. Further modification using a gold coating was found to enhance cellular adhesion, orientation and organization within these micro-/nano-stripes, which consequently prevented excessive adhesion of smooth muscle cells (SMCs) to the thin PEG ridges, thereby effectively confining the cells to the Fe$_3$O$_4$-laid channels. This architectural design promotes the alignment of the cytoskeleton and elongation of actin filaments, leading to the organized formation of muscle bundles and a tendency for SMCs to adopt synthetic phenotypes. Muscle patches are harvested from the micro-/nano-stripes and transplanted into a rat esophageal defect model. *In vivo* experiments demonstrate the exceptional viability of these muscle patches and their ability to accelerate the regeneration of esophageal tissue. Overall, this study presents an efficient strategy for constructing muscle patches with directional alignment and muscle bundle formation of SMCs, holding significant promise for muscle tissue regeneration.

1. Introduction

Muscle tissue serves indispensable roles within the various tissues and organs of the human body. For instance, the muscular contractions in the digestive tract are primarily responsible for propelling food [1], while vascular smooth muscles regulate blood vessel tone and contraction [2]. However, injuries, infections and severe diseases can cause muscle atrophy, functional decline or even complete loss [3]. Since muscle cells possess limited regenerative capacity as terminally differentiated cells, traditional clinical approaches like drug therapy, physical

exercise, or nutritional interventions face significant challenges in effectively repairing muscle tissue [4,5]. The development of engineered muscle patches presents a compelling solution for muscle replacement and regeneration [6] and holds the potential to address issues associated with muscle repair, offering robust tools to restore muscle function effectively.

Muscle tissues primarily consist of muscle fibers organized into bundles, and their precise alignment is essential for generating contraction force [7]. To mimic this natural structure, engineered muscles must attain cellular-level consistency in their orientation, and to

---

* Corresponding author.
** Corresponding author. Health Science Center, Ningbo University, Ningbo, 315211, China.
*** Corresponding author.
E-mail addresses: yanglu@nbu.edu.cn (L. Yang), zhanghua@nbu.edu.cn (H. Zhang), zhuyabin@nbu.edu.cn (Y. Zhu).
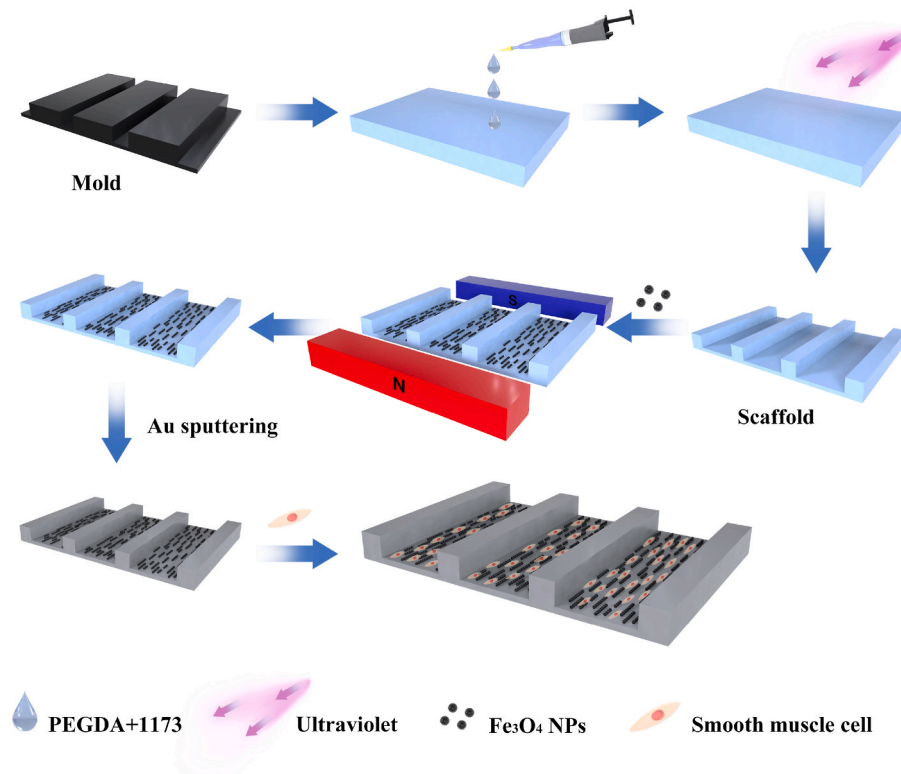[1] These authors contributed equally to this work.

Fig. 1. Schematic diagram of scaffold preparation and induction of cell orientation.

this end, tissue engineering scaffolds serve as a pivotal strategy for achieving proper cell orientation [8]. A well-designed biological scaffold not only promotes cell proliferation and orientation *in vitro* but also facilitates *in vivo* repair [9,10]. For instance, Kobayashi et al. [11] reported that orthogonally oriented scaffolds with aligned fibers could effectively guide cell growth along these fibers. Similarly, Choi et al. [12] successfully generated a layer of vascular smooth muscle cells (SMCs) using a circular arrayed structure within a microfluidic channel.

In our previous research work, we engineered a biodegradable scaffold containing microchannels using crosslinked poly(ester urethane) (CPU) and silk fibroin (SF) as the constituent materials to provide support for the directed growth and proliferation of SMCs [13]. Subsequently, we utilized this scaffold with microchannel patterns to construct a bilayered muscle tissue model, comprising inner-circular and outer-longitudinal layers, to promote the regeneration of esophageal smooth muscles [14,15]. These research efforts confirmed that the specific channel structures and aligned fibers within the scaffold were indeed effective in inducing cell orientation.

In this present study, we introduced aligned chain-like assemblies of Fe_3O_4 onto a micropatterned poly(ethylene glycol) (PEG) substrate to facilitate cellular orientation and organization. The matrix for this construct, (ethylene glycol) diacrylate (PEGDA), was used to form the microchannel pattern with the assistance of a silicon mold. To create aligned stripes within these micro-/nano-stripes, we coated Fe_3O_4 magnetic nanoparticles (Fe_3O_4 NPs) onto the channels using directional N/S magnetic fields. Further modification with a gold coating enhances cellular adhesion, orientation and organization in these micro-/nano-stripes, allowing the primary SMCs to grow along the direction of micro-/nano-stripes., following which a muscle patch was obtained. To investigate the biological function and mechanisms underlying these muscle patches, RNA sequencing analysis was conducted, and the results revealed that although the muscle patches exhibited weaker contractile abilities, they demonstrated stronger capabilities in terms of "Cell migration" and "Wound healing" compared to normal tissues. These findings were consistent with expectations, as some SMCs within the

muscle patch tended to display a synthetic phenotype, although some retained their contractile characteristics. Furthermore, *in vivo* experiments confirmed that the muscle patches accelerated the repair of esophageal muscle defects in rats. Overall, these findings highlight the potential therapeutic value of our proposed engineered muscle patches in treating muscle-related disorders.

2. Materials and methods

2.1. Materials

PEGDA and Fe_3O_4 magnetic nanoparticles (Fe_3O_4 NPs, 100–200 nm) were purchased from Shanghai Macklin Biochemical Co., Ltd. (China). Photoresist reagent (AZ5214) was obtained from MicroChemicals GmbH (Germany), and positive colloid developer (RZX-3038) was purchased from Suzhou Ruihong Electronic Chemicals Co., Ltd. (China). 2-Hydroxy-2-methylpropiophenone was obtained from Shanghai Aladdin Biochemical Technology Co., Ltd (China).

Anti-α-smooth muscle actin (α-SMA) rabbit antibody, 594-conjugated anti-vimentin antibody, anti-recombinant actinin alpha 2 (ACTN2) rabbit antibody, anti-Desmin mouse antibody, anti-Osteopontin (OPN) rabbit antibody and goat anti-rabbit IgG (Alexa Fluor® 594) were purchased from Proteintech Group, Inc. (USA). Antibodies of anti-Ki67 (rabbit) and anti-α-SMA (mouse) were obtained from Affinity Biosciences (USA). Goat anti-mouse IgG (Alexa Fluor® 488) and goat anti-rabbit IgG (Alexa Fluor® 647) were bought from Abcam Co., Ltd (UK), TRITC Phalloidin from Solarbio Science & Technology Co., Ltd (China), and the lentivirus used in this study was transfected by ZsGreen fluorescent protein and purchased from Tsingke Biotechnology Co., Ltd. (China).

2.2. Construction and characterization of the mold patterned with microchannels

The mold was prepared by photolithography and etching

technology. First, the monocrystalline silicon wafer (12×12 mm^2) was sequentially cleaned with acetone, isopropanol and deionized water using an ultrasonic process (power of 100 W) for 10 min, followed by drying with nitrogen gas and then baking on a hot plate (180 °C) for 10 min. Next, a layer of photoresist AZ5214 was spin-coated onto the silicon wafer at 3000 rpm for 60 s, baked at 95 °C for 10 min, and exposed to ultraviolet light using a customized lithography mask and an ultraviolet lithography machine (URE-2000B, China). After exposure, it was developed in a positive colloid developer and rinsed with deionized water. Finally, the developed wafer was dried on a hot plate at 120 °C for 2 min. The etching process was conducted using an Inductively Coupled Plasma Etcher (Plasmapro100Cobra180, UK) with octafluorocyclobutane (C_4F_8) as the passivation gas and sulfur hexafluoride (SF_6) as the etching gas. The microchannels on the silicon wafer's surface were observed using an electron beam lithography machine (eLINE Plus, Raith GmbH, Germany).

2.3. Preparation and characterization of PEG scaffold

PEGDA was selected as the scaffold matrix and applied to the mold to create a specific surface structure. To achieve this, PEGDA was blended with 2-hydroxy-2-methylpropiophenone at a ratio of 200:1 (v/v) to form a homogeneous solution, which was then poured onto the silicon mold and cured for 80 s under ultraviolet light with a power of 100 W. This process resulted in the scaffold with microchannels on its surface. The morphology of the scaffold was examined using laser confocal scanning microscopy (OLS5000, Olympus Corporation, Japan).

2.4. Modification of PEG scaffold with Fe₃O₄ micro-/nano-stripes (PEGM)

Fe₃O₄ NPs aqueous solution (50 μL) was applied onto the scaffold, which was positioned within a linear magnetic field created by North (N) and South (S) magnets. The Fe₃O₄ NPs were immediately attracted into the channels and aligned into micro-/nano-stripes due to the magnetic force. Following the evaporation of water from the Fe₃O₄ NPs solution at room temperature, a thin layer of gold was evenly deposited onto the scaffold using an Ion Sputter Coater (ISC 150, China) to immobilize the Fe₃O₄ micro-/nano-stripes and enhance the biocompatibility of the substrate. The scaffold's distinct structures with varying densities of Fe₃O₄ micro-/nano-stripes were observed using a scanning electron microscope (SEM, Phenom Pro, China). Energy Dispersive Spectroscopy (EDS) analysis of micro-/nano-stripes on PEGM scaffolds were obtained on SEM (ZEISS Sigma 300, Germany). The imaging and analysis were performed at 15 kV. Maps of elements Fe, O and Au were acquired for each sample. The surface topography and roughness were investigated on Atomic Force Microscopy (AFM, Bruker Dimension Icon, Germany) in tapping mode using silicon cantilevers (spring constant: 40 N/m, resonant frequency: 300 kHz). To assess the stability of the Fe₃O₄ micro-/nano-stripes on the PEG scaffold, we measured the line length before and after the PEG scaffold underwent swelling. The preparation process of the PEGM scaffold is illustrated schematically in Fig. 1.

2.5. Extraction and identification of SMCs

Primary SMCs were isolated from the lower one-third of rats' esophageal muscularis. First, the muscle tissue was cut into small pieces and placed in Dulbecco's modified Eagle's medium (DMEM) supplemented with 10 % fetal bovine serum (FBS) and 1 % penicillin-streptomycin. The culture was maintained at 37 °C in an environment containing 5 % CO_2. After 5 days, cells migrated out of the tissue fragments. Then, the tissue fragments were removed, and the cells were subcultured.

To confirm the identity of the cells following *in vitro* culture, immunofluorescent (IF) staining was performed. The cells were rinsed with PBS, fixed in 4 % paraformaldehyde for 15 min, permeabilized with

0.2 % Triton X-100 and blocked with 3 % bovine serum albumin (BSA) for 1 h. Overnight incubation at 4 °C with anti-α-SMA mouse antibody (1:200) and 594-conjugated vimentin antibody (1:200) was performed, after which the cells were exposed to goat anti-mouse IgG (1:500, Alexa Fluor® 488) for 1 h. The nuclei were stained with 4′,6-diamidino-2-phenylindole (DAPI), and cell identity was confirmed by observing their morphology under an inverted fluorescence microscope (DMi8, Leica, Germany).

2.6. SMCs orientation and elongation on PEGM scaffold

A total of 5×10^4 SMCs were seeded on culture plates (Normal), PEG (Control) and PEGM scaffold (prepared with 0.5 or 1 mg/mL Fe₃O₄ NPs, named as PEGM0.5 or PEGM1.0, respectively). After culturing for 24 h, the cells were stained by IF. The cells were permeabilized and blocked with 0.2 % Triton X-100 and 3 % BSA for 1 h, followed by incubation with anti-α-SMA mouse antibody (1:200) for 2 h at room temperature. Subsequently, the cells were incubated with goat anti-mouse IgG (1:500, Alexa Fluor® 488) for 1 h. F-actin was labeled with TRITC Phalloidin after a 30-min incubation at room temperature, and cell nuclei were stained with DAPI. Cell morphology was assessed using a confocal microscope (STELLARIS 5, Leica, Germany).

The elongation of SMCs on different substrates was quantified using the aspect ratio, defined as the ratio of the long axis to the short axis across cell nuclei.

2.7. Constitution of muscle patch

Primary esophageal SMCs were transfected with lentivirus marked with ZsGreen fluorescent protein (80 μL, 1.0×10^8 virus/mL). The lentivirus was added to a T25 cell culture bottle containing 4 mL of medium when the cells reached 50 % confluence. After 24 h, the medium was replaced with a culture medium without lentivirus. When the cells reached confluence, they were detached using 0.25 % trypsin (700 μL) and then seeded onto PEGM0.5 to construct a smooth muscle patch. Specifically, a 2 mL cell suspension (2.5×10^5 cells/mL) was added to the scaffold, which was placed in a 24-well cell culture plate and incubated at 37 °C in an environment with 5 % CO_2 and humid air. The culture medium, consisting of DMEM supplemented with 10 % FBS and 1 % penicillin-streptomycin, was changed every other day. On day 8, SMCs with the same density were reseeded to expedite cell growth and fusion. The orientation of esophageal SMCs and the development of muscle tissue were observed using inverted fluorescent microscopy.

2.8. Histological analysis and functional detection of the muscle patch

The constructed muscle patch was sectioned into slices at a thickness of ∼6 μm using a frozen microtome (CryoStarTM NX50, Thermo Scientific, USA), then stained following the instructions provided by the Hematoxylin & Eosin (H&E) kit and Masson's Trichrome staining kit (Yuanye, China). IF staining was also performed to assess the expression of α-SMA to confirm SMC differentiation during tissue formation. For IF staining, the tissue slices were permeabilized and blocked using Triton X-100 (0.2 %) and bovine serum albumin (BSA, 3 %, Solarbio Life Sciences, China) for 1 h. Subsequently, they were incubated overnight at 4 °C with anti-α-SMA rabbit antibody (1:200), followed by a 1-h incubation with goat anti-rabbit IgG (1:500, Alexa Fluor® 594). Cell nuclei were stained with DAPI. The tissue morphology and staining were examined using an inverted fluorescence microscope.

The generation of action potentials is essential for muscle contractile function. Herin, we utilized a multi-channel electrophysiological mapping system (MappingLab EMS64, USA) to measure action potentials. Briefly, the muscle patch was positioned on the electrode platform, and the system automatically recorded the time-dependent changes in electrical signals (resting potential). Subsequently, we applied acetylcholine (ACH, 0.1 %, w/v, 50 μL) onto the patch, and the resulting
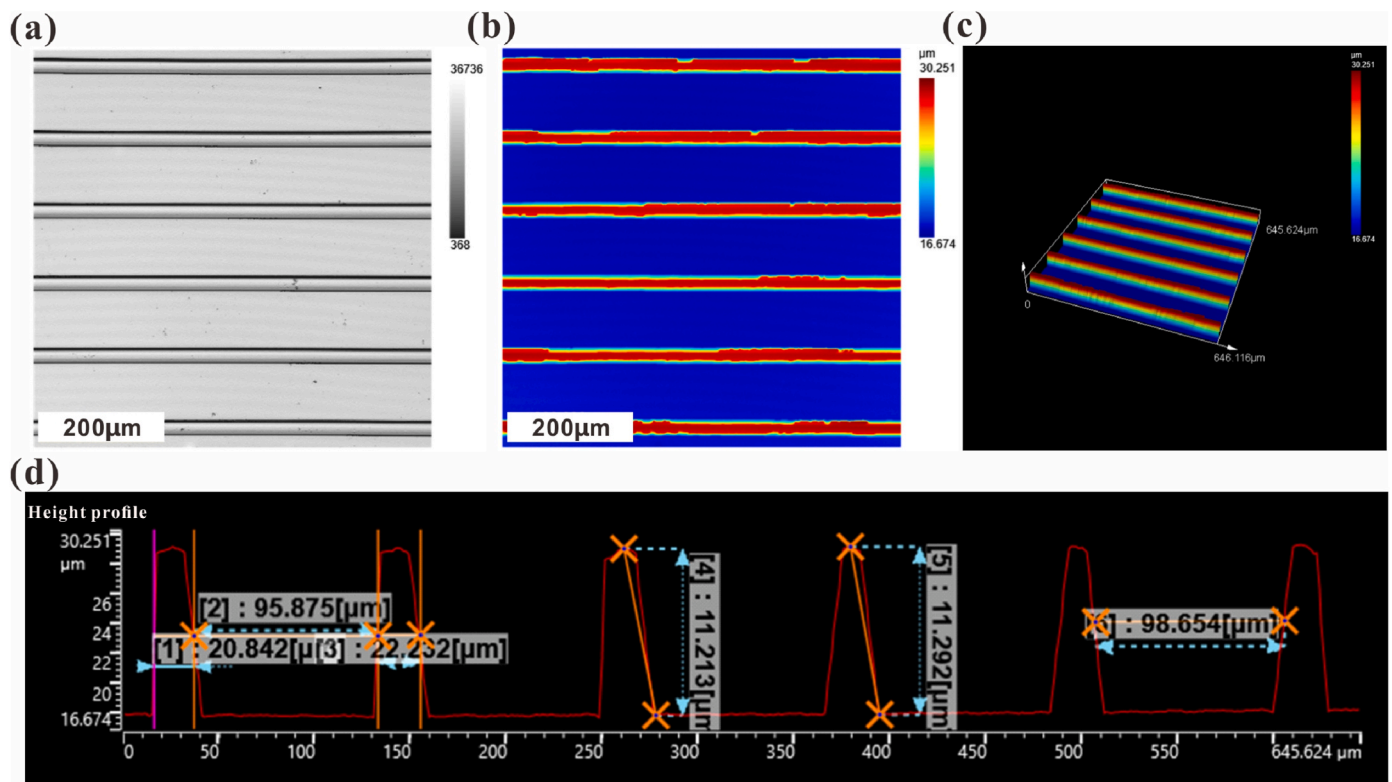
Fig. 2. Characterization of the PEG scaffold. (a) Surface morphology, (b) apparent topological structure, (c) 3D structure and (d) size measurement under 3D laser confocal microscopy.

electrical signals were recorded using the same methodology.

2.9. RNA sequencing and analysis

Total ribonucleic acid (RNA) was extracted from both the rat esophageal muscle and the engineered muscle tissues (cells derived from the same rat) following the protocol provided in the Total RNA Extraction Reagent kit (RNAiso Plus, TAKARA). The purity and concentration of the extracted RNA were determined using a NanoDrop 2000 spectrophotometer (Thermo Scientific, USA). Additionally, RNA integrity was assessed using the Agilent 2100 Bioanalyzer (Agilent Technologies, USA). Library preparation was performed using the VAHTS Universal V6 RNA-seq Library Prep Kit in accordance with the manufacturer's instructions. Transcriptome sequencing and subsequent analysis were conducted by OE Biotech Co., Ltd. (Shanghai, China).

2.10. The phenotype of SMCs on the PEGM0.5 scaffold

A total of 3×10^4 SMCs were seeded on culture plates (Normal) and PEGM0.5 scaffold. IF staining was employed to assess the expression of Desmin and OPN to confirm the phenotypic conversion of SMCs. After 24 and 48 h of culture, the SMCs were permeabilized and blocked using 0.2 % Triton X-100 and 3 % BSA, respectively, for 1 h. Subsequently, the cells were incubated with anti-Desmin mouse antibody (1:400) and anti-OPN rabbit antibody (1:150) for 2 h at room temperature, followed by a 1-h incubation with goat anti-mouse IgG (1:500, Alexa Fluor® 488) and goat anti-rabbit IgG (1:500, Alexa Fluor® 647). F-actin was labeled with TRITC Phalloidin after a 30-min incubation at room temperature, and the cell nuclei were stained with DAPI. The localization and expression of Desmin and OPN were observed using a confocal microscope.

2.11. In vivo tests

The animal experiment protocol received approval from the Animal Ethics and Welfare Committee (AEWC) of Ningbo University. Institutional animal ethics approval was obtained before commencing the experiments (approval number: 12,238). Male Sprague Dawley (SD) rats aged 6 weeks were purchased from Beijing Charles River Experimental Animal Technology Co., Ltd. (China) and divided into two groups: experimental and control (n = 5). Under isoflurane anesthesia, a defect length of ~0.4 cm was created in the rat esophageal muscle tissue. Autologous cells were used to construct the muscle patch and further replaced the damaged muscles. The tissue was sutured using biological glue (Jitian Bio, China), and the skin was subsequently sutured. For the control group, the same procedure was followed, but no muscle patch replacement was performed. On postoperative days 1, 3, or 5, the rats were anesthetized, and the operated tissue was exposed for histological analysis. IF staining was conducted using antibodies against Ki67, α-SMA and ACTN2 to monitor the wound healing process.

### 2.12. Statistics

The data are presented as means ± standard deviation (SD). Statistical comparisons between two groups were performed using Student's t-test, while differences among multiple groups were assessed using the one-way ANOVA method. A significance level of $p < 0.05$ was considered statistically significant, with *** indicating $p < 0.001$ and **** indicating $p < 0.0001$.

3. Results

3.1. Characterization of the mold

The silicon mold was constructed using photolithography and etching techniques, and its topography was examined using an electron beam lithography machine. As shown in Fig. S1, the master mold featured microchannels with a width of approximately ~20 μm, separated by walls measuring approximately ~100 μm in width and ~11 μm
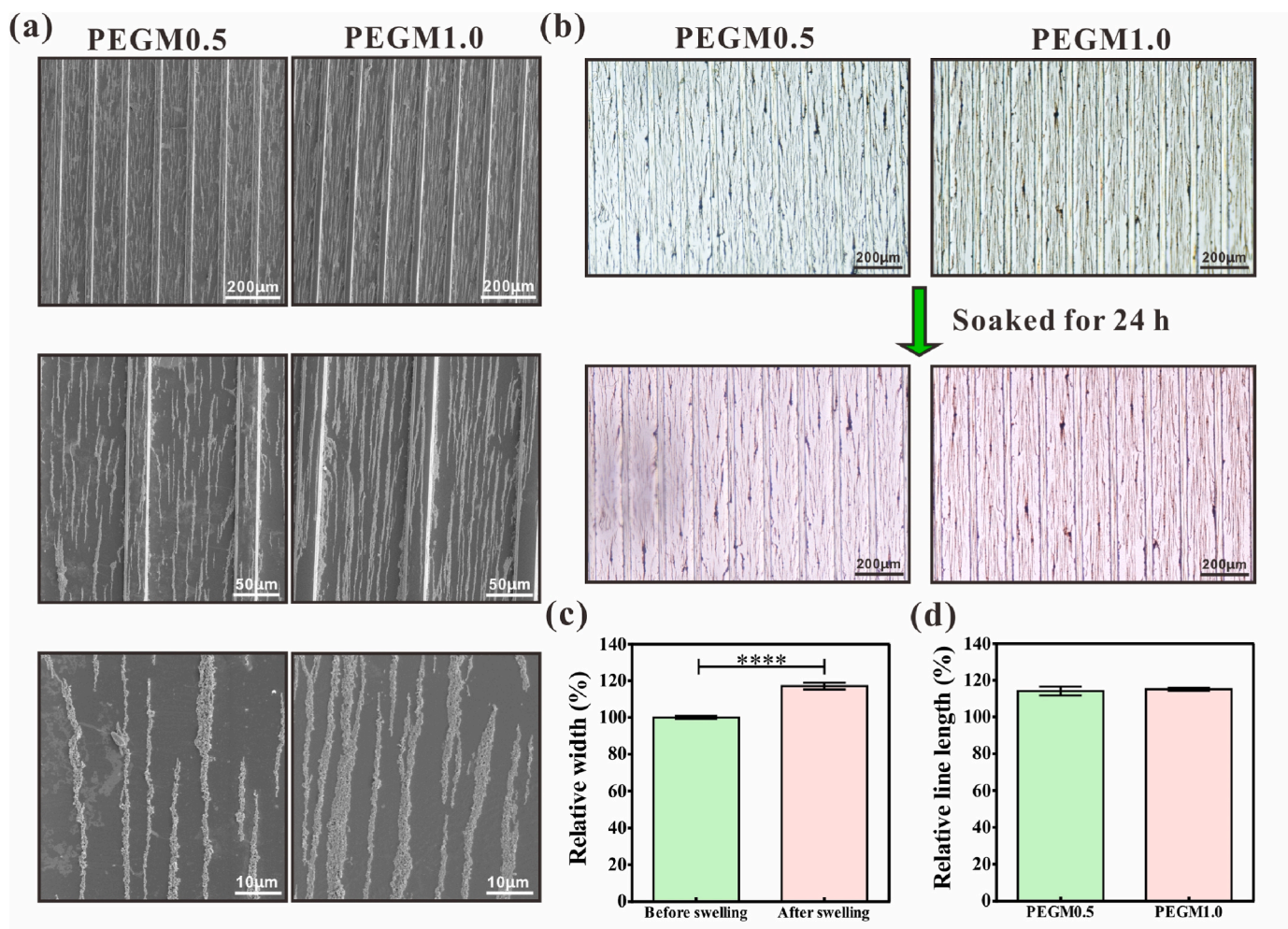
Fig. 3. Characterization of magnetic Fe_3O_4 NPs modified scaffold. (a) The apparent structure of PEGM0.5 and PEGM1.0 under SEM. (b) The structure of PEGM0.5 and PEGM1.0 before and after swelling. (c) Relative width of microchannel before/after swelling. (d) Relative length of Fe_3O_4 micro-lines on the scaffold after swelling (compared with the length before swelling).

in depth.

3.2. Characterization of the PEG scaffold

A PEGDA solution was applied to the mold to replicate its specific structure. As shown in Fig. 2a and b, a well-defined topological structure with dimensions of approximately ~100 μm in width, ~20 μm in spacing and ~11 μm in depth was achieved. The three-dimensional structure is presented in Fig. 2c, and size measurements were conducted using 3D laser confocal microscopy (Fig. 2d). The observations indicated that our protocol successfully produced a PEG scaffold with the desired structures. These engraved microchannels provide an adequate pattern for cell growth and orientation.

3.3. Characterization of PEGM scaffold

To effectively guide the alignment of SMCs, we modified the channel-patterned scaffold with Fe_3O_4 NPs and directed their formation into micro-/nano-stripes using magnetic fields, followed by fixation with gold sputtering. The apparent structure of PEGM was observed under SEM, which revealed that the concentration of Fe_3O_4 NPs was positively correlated with the density and width of the micro-/nano-stripes (Fig. 3a). EDS elemental maps showed that the gold uniformly deposited onto the PEG substrate (Figs. S2 and S3). The surface topography and roughness were further investigated by AFM (Fig. S4). The

results showed that the micro-/nano-stripes on PEGM1.0 have a bigger width and height than those on PEGM0.5, which might be attributed to the more magnetic Fe_3O_4 NPs on PEGM1.0 than on PEGM0.5.

We also investigated the swelling properties of PEGM, and the results showed that the PEGDA matrix expanded by approximately ~160 % compared to the original material after immersion in water for 24 h (Fig. S5). To assess the stability of Fe_3O_4 micro-/nano-stripes on the scaffold, PEGM0.5 and PEGM1.0 were soaked in the culture medium for 24 h, respectively. The results indicated that the integrity of the micro-/nano-stripes remained unchanged, as observed under an optical microscope (Fig. 3b). Although the width of micro-channels expanded slightly, from 100 % to ~117 %, after swelling (Fig. 3c), the length elongated to ~114 % for PEGM0.5 and ~115 % for PEGM1.0, respectively (Fig. 3d). These findings suggest that the micro-/nano-stripes may undergo slight expansion and elongation with the swelling of the PEG matrix but do not compromise the scaffold's topography. Therefore, PEGM demonstrates stability in the culture medium.

3.4. SMCs orientation and elongation on PEGM scaffold

Primary esophageal SMCs were cultured and identified based on the expression of α-SMA and Vimentin (Fig. S6). When SMCs were seeded onto various substrates, distinct orientation states were observed. The cells exhibited a growing state with an alignment tendency on scaffolds PEG (Control), PEGM0.5 and PEGM1.0 but displayed random
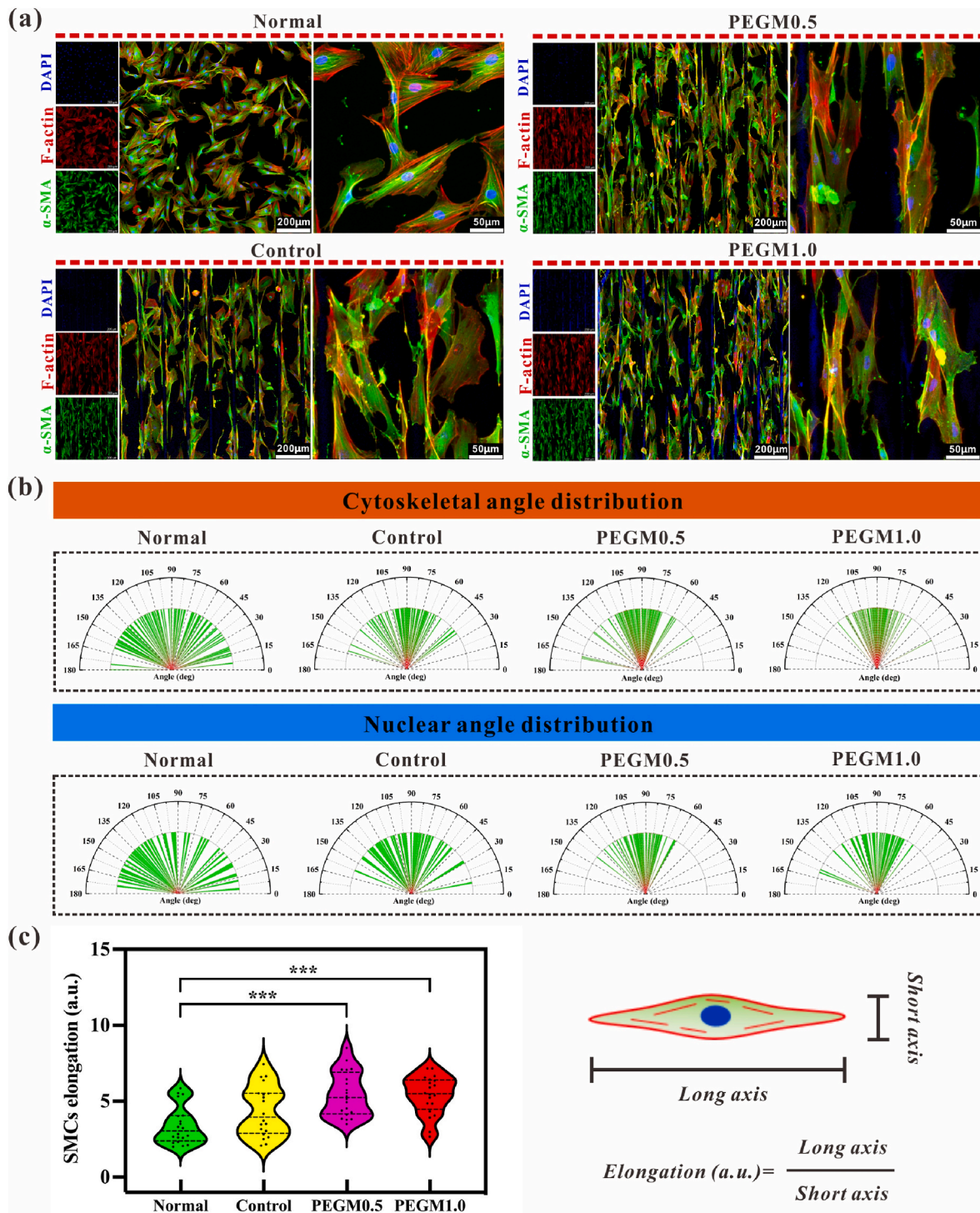
Fig. 4. Cell orientation performance on different substrates. (a) Observation of the SMCs orientation on different substrates after IF staining. SMCs were seeded on culture plates (Normal), PEG scaffold (Control), PEGM0.5 and PEGM1.0 for 24 h. (b) Statistical distribution of cytoskeletal angle and nuclear angle. (c) Statistical data of SMCs elongation.

orientation on culture plates (Normal) (Fig. 4a). The distributions of cytoskeletal angle and nuclear angle revealed that cells exhibited superior orientation on PEGM scaffolds compared with PEG scaffolds. However, there was little difference in the orientation performance of cells on PEGM0.5 and PEGM1.0 (Fig. 4b). The elongation of SMCs increased with improved orientation properties, and no statistically significant difference was observed between cells on PEGM0.5 and PEGM1.0 (Fig. 4c). Taken together, PEGM induced directional alignment of SMCs, with PEGM0.5 being the preferred choice due to its Fe_3O_4

micro-line distribution and favorable SMC behavior. Thus, PEGM0.5 was selected for subsequent experiments.

3.5. Histological analysis and functional detection of the engineered muscle patch

SMCs were transfected with Zsgreen fluorescent protein and seeded onto PEGM0.5. As shown in Fig. 5a, SMCs successfully adhered to the scaffold and grew with consistent orientation. The number of green
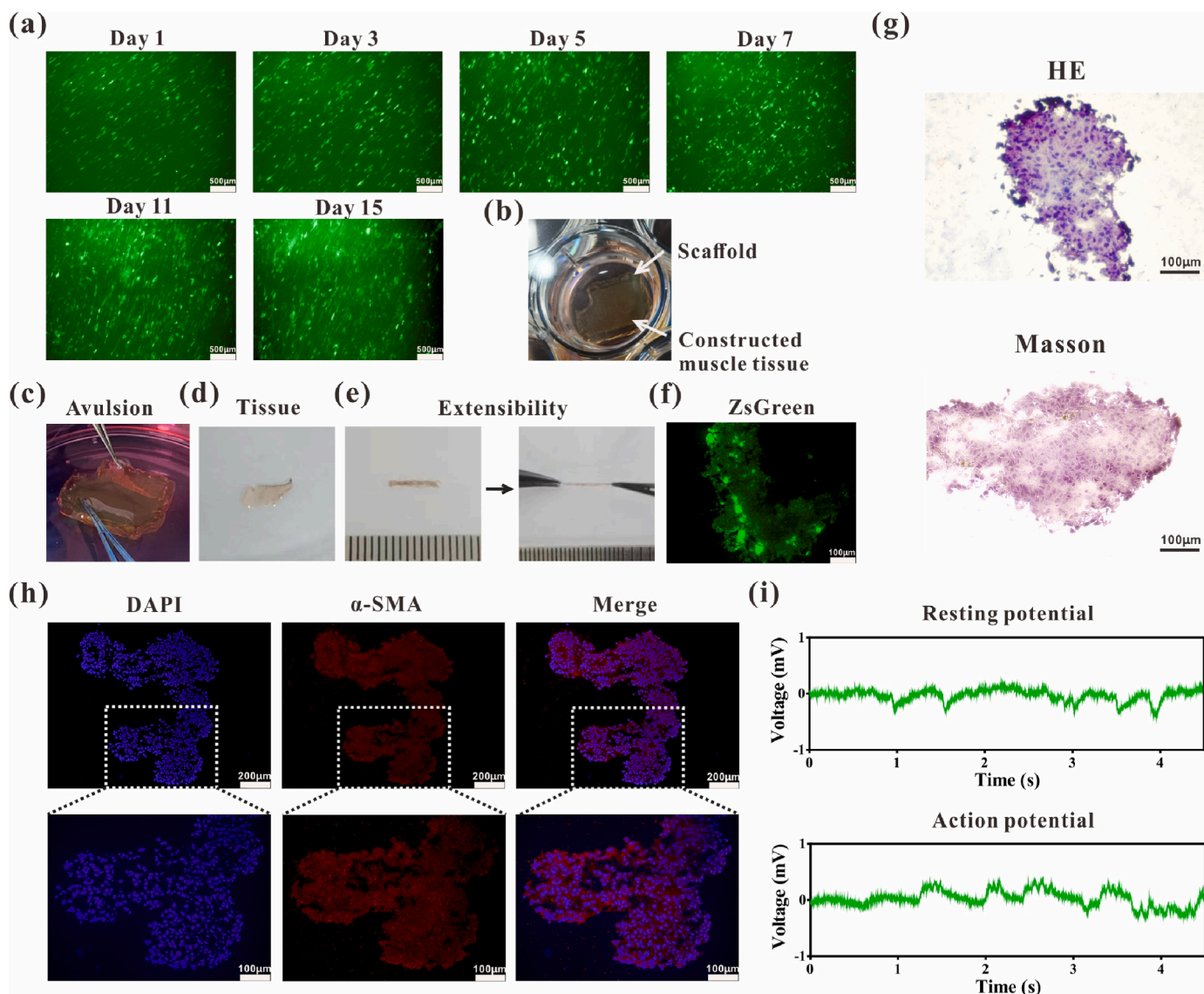
Fig. 5. Construction, histological analysis and function detection of the muscle patch. (a) Seeding and formation of smooth muscle patch. (b) Appearance of muscle patch on scaffold, cultured for 15 days. (c) The avulsion process. (d) Appearance of the muscle patch. (e) Detection of the muscle patch stretching property. (f) Observation of the muscle patch under fluorescence microscopy. The patch was cut into slices on frozen microtome at ~6 μm. (h) Observation of α-SMA expression of the muscle patch. (g) Staining with H&E and Masson's trichome. (i) Measurements of the resting and action potentials of the muscle. The muscle tissue was tiled on the electrodes to record the data.

fluorescent cells increased over time, indicating robust SMC proliferation on the scaffold. By day 8, the SMCs were seeded again at the same density to accelerate muscle tissue formation. By day 15, multiple SMC layers had formed, visible as a distinct muscle patch (Fig. 5b). The muscle patch exhibited a beige and translucent appearance and could be easily detached from the scaffold (Fig. 5c and d), and the cells within the patch exhibited oriented growth.

The muscle patch displayed compactness and stretchability, indicating successful tissue formation (Fig. 5e). When stained with a fluorescent dye, the tissue emitted green fluorescence at 488 nm excitation light after being sectioned using a frozen microtome (Fig. 5f). Tissue morphology and collagen fibers were assessed using H&E and Masson's trichrome staining. The results revealed matrix filling within the tissues (Fig. 5g, H&E), although there was limited collagen content in the matrix, likely due to the relatively short culture time that did not allow sufficient collagen secretion (Fig. 5g, Masson). Immunofluorescent staining for α-SMA confirmed that primary SMCs maintained their muscle characteristics after 15 days of *in vitro* culture (Fig. 5h). Overall,

these results showed that we successfully constructed an *in vitro* smooth muscle patch using a Fe_3O_4-modified scaffold.

The generation of action potential is a prerequisite for muscle contractile function. Action potential was assessed using a multi-channel electrophysiological mapping system. When the muscle patch was placed on the electrode platform, an irregular negative potential was recorded (Fig. 5i, resting potential), indicating the viability of the constructed muscle. Upon application of ACH solution to the muscle, continuous and regular action potentials were generated (Fig. 5i, action potential). Surprisingly, the *in vitro* constructed muscle could generate action potentials in response to ACH stimulation. Thus, we conclude that the engineered muscle is active and possesses the capability for action potential generation.

3.6. RNA sequencing and analysis

To determine the biological mechanisms underlying the engineered muscle, transcriptome sequencing was conducted to assess the
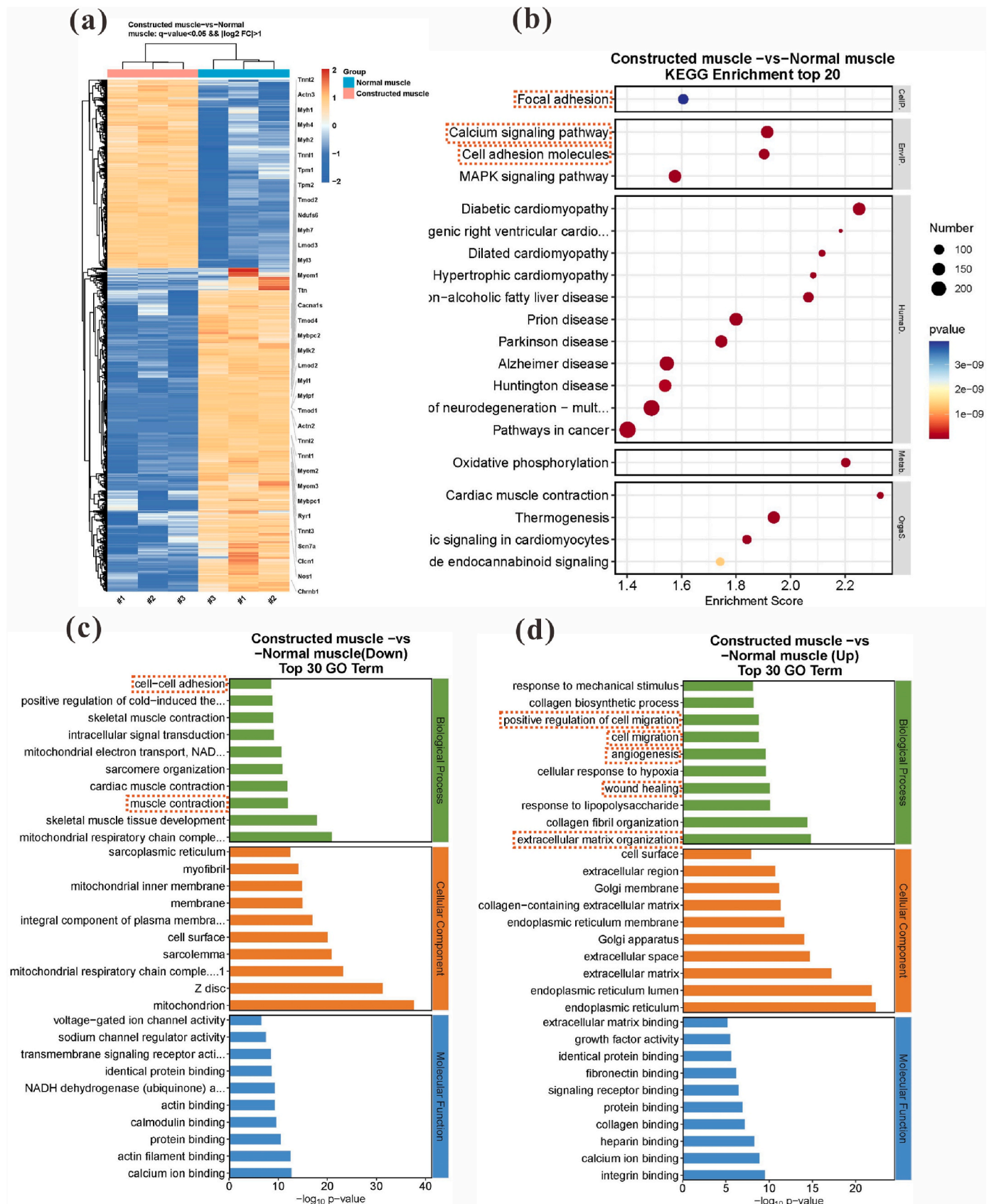
Fig. 6. RNA sequencing and analysis. (a) Screening and presentation of the DEGs. (b) KEGG enrichment analysis. (c) GO enrichment analysis for down-regulated DEGs and (d) up-regulated DEGs.
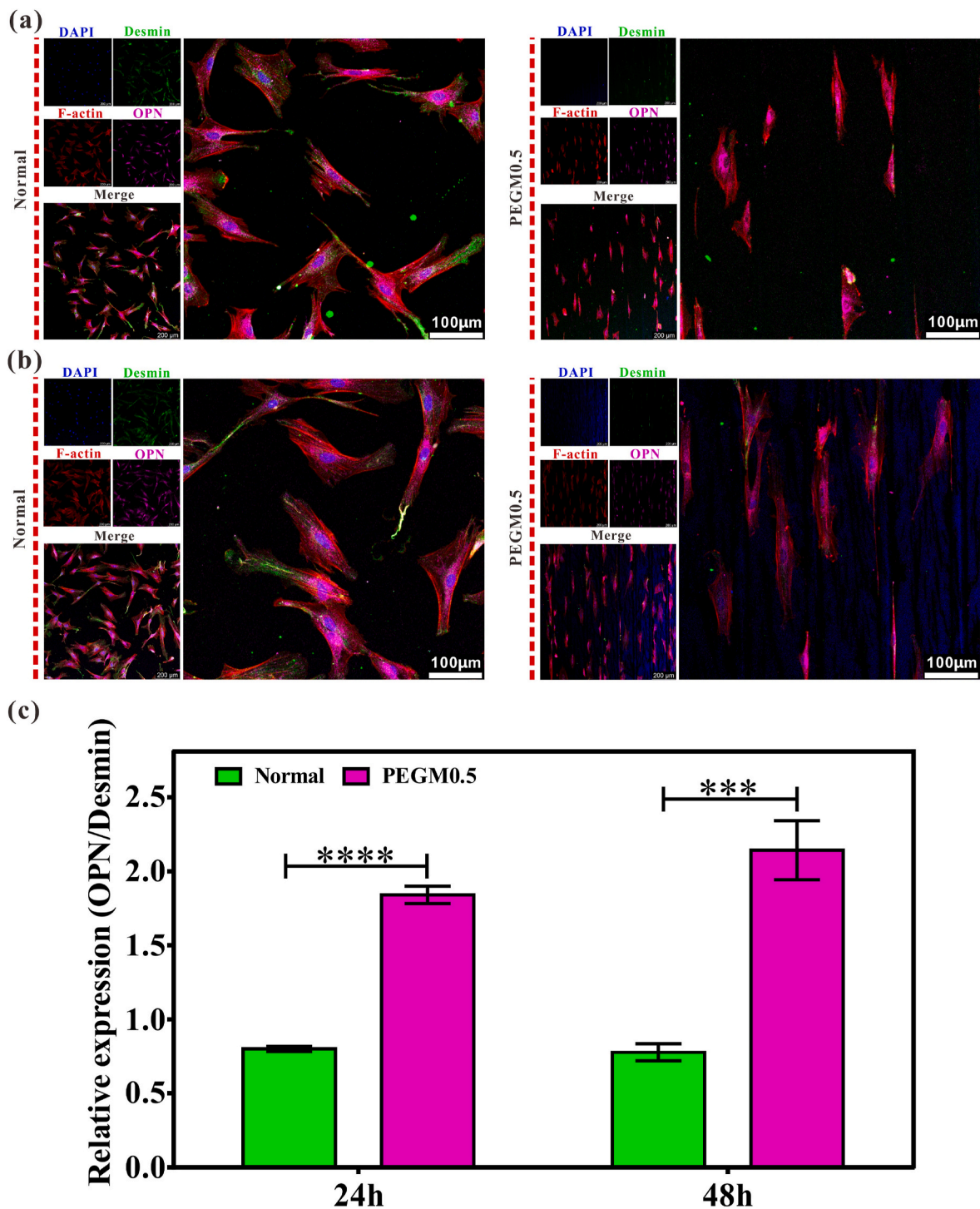
Fig. 7. The phenotype of SMCs on PEGM0.5 scaffold. Expression of Desmin (green), F-actin (red) and OPN (purple) in SMCs on different substrates after culture for (a) 24 h and (b) 48 h. (c) Relative expression of OPN/Desmin in SMCs on different substrates after culture for 24 h and 48 h. (For interpretation of the references to color in this figure legend, the reader is referred to the Web version of this article.)

differentially expressed genes (DEGs) between the constructed muscle and normal esophageal muscle based on the criteria of "q-value <0.05 & |Log$_2$ FC| > 1" (Fig. 6a), and their functional enrichment was analyzed [16]. Notably, the Kyoto Encyclopedia of Genes and Genomes (KEGG) analysis indicated that these genes were associated with the "Calcium signaling pathway," which is pertinent to muscle contraction (Fig. 6b). Gene Ontology (GO) analysis of down-regulated differential genes revealed differences in the biological process related to "Muscle contraction" (Fig. 6c). These findings suggest that the contractile

function of the constructed muscle patch may be lower than that of normal muscle tissue. Furthermore, GO analysis of up-regulated differential genes showed enrichment in biological processes such as "Cell migration", "Angiogenesis", "Wound healing" and "Extracellular matrix organization" (Fig. 6d), indicating that the constructed muscle is conducive to addressing diseases characterized by muscle defects or incapability.

The observed weak contractile ability but strong capabilities in "Cell migration" and "Wound healing" appear to be linked to the phenotypic
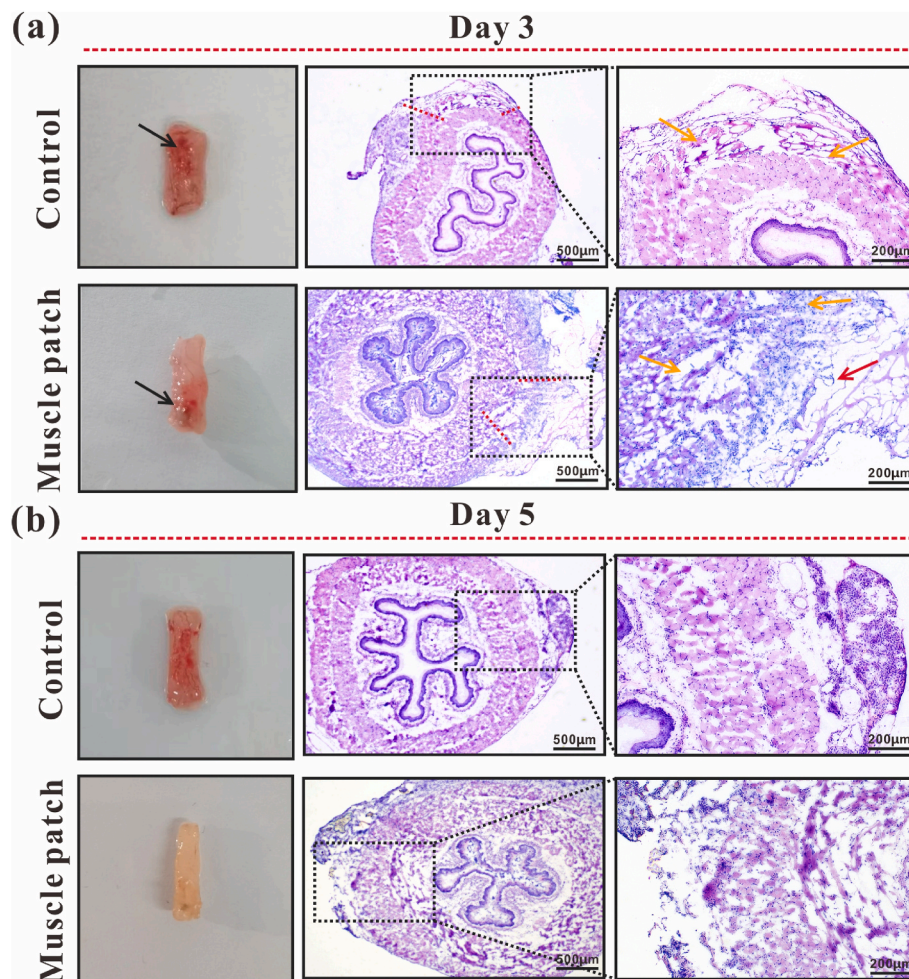
Fig. 8. Regeneration of esophageal muscles after muscle patch transplantation in a defective esophagus model (~0.4 cm in length was defective). Wound appearance and H&E staining at day 3 (a) and day 5 (b), with self-repair of the defected muscle layer as the control. Black arrows refer to the location of the regenerating muscle, which was exhibited between the red dotted lines in H&E staining images; Red arrows refer to the biological glue and orange arrows direct to the migrating SMCs. (For interpretation of the references to color in this figure legend, the reader is referred to the Web version of this article.)

transformation of SMCs between the contractile and synthetic types [17]. Synthetic SMCs exhibit a higher growth rate and enhanced migration activity but lower contraction ability compared to contractile SMCs. Importantly, these SMC phenotypes are reversible and influenced by the extracellular environment [18,19]. Based on the RNA sequencing data, we hypothesize that some cells within the patches may tend towards a synthetic phenotype. This shift could be advantageous, to some extent, for muscle tissue repair, as reflected in the observed up-regulation of genes associated with "Cell migration," "Wound healing," and "Extracellular matrix organization" in the GO analysis of up-regulated differential genes (Fig. 6).

3.7. The phenotype of SMCs on PEGM0.5 scaffold

To further validate the phenotype of SMCs cultured on the PEGM0.5 scaffold, we assessed the expression of Desmin and OPN using IF. OPN serves as a specific marker for the synthetic phenotype of SMCs, while Desmin indicates the contractile phenotype. We used relative expression levels (OPN/Desmin) as a metric to gauge the inclination of SMCs towards synthetic phenotypes. The results revealed varying levels of Desmin and OPN expression in SMCs grown on different substrates. After 24 h, both proteins were abundantly expressed in SMCs cultured on a culture plate. Conversely, SMCs seeded on PEGM0.5 primarily expressed OPN and exhibited minimal Desmin expression (Fig. 7a). A similar pattern was observed in SMCs on these substrates after 48 h

(Fig. 7b). Importantly, SMCs cultured on PEGM0.5 displayed a higher relative expression level (OPN/Desmin) compared to those on the culture plate (Fig. 7c), indicating that some SMCs on PEGM0.5 exhibited a stronger inclination toward synthetic phenotypes than their counterparts on the culture plate.

3.8. In vivo regeneration of muscle tissue

The rat esophagus comprises three muscle layers, namely the outer, inner, and mucosal muscularis, arranged from outermost to innermost (Fig. S7). To assess the efficacy of the smooth muscle patches in tissue repair, we conducted an animal experiment involving SD rats with esophageal muscle defects, which were subsequently repaired using the engineered muscle patches. The results revealed that the initial stages of muscle tissue repair in the rat esophagus primarily relied on the proliferation and migration of peripheral muscle cells when no materials were used to replace the defective muscle (Fig. 8a, Control, indicated by orange arrows). Over time, muscle growth occurred, accompanied by the formation of fresh granulation tissue around the muscle layer (Fig. 8b, Control).

Conversely, when the defect was filled with our engineered muscle patch, the patch occupied the defective site, and the muscle cells initially dispersed towards the periphery to cover the defect on the first day (Fig. S8a, indicated by green arrow). Ki67, a protein expressed by proliferating cells [20], served as a survival indicator for the engineered
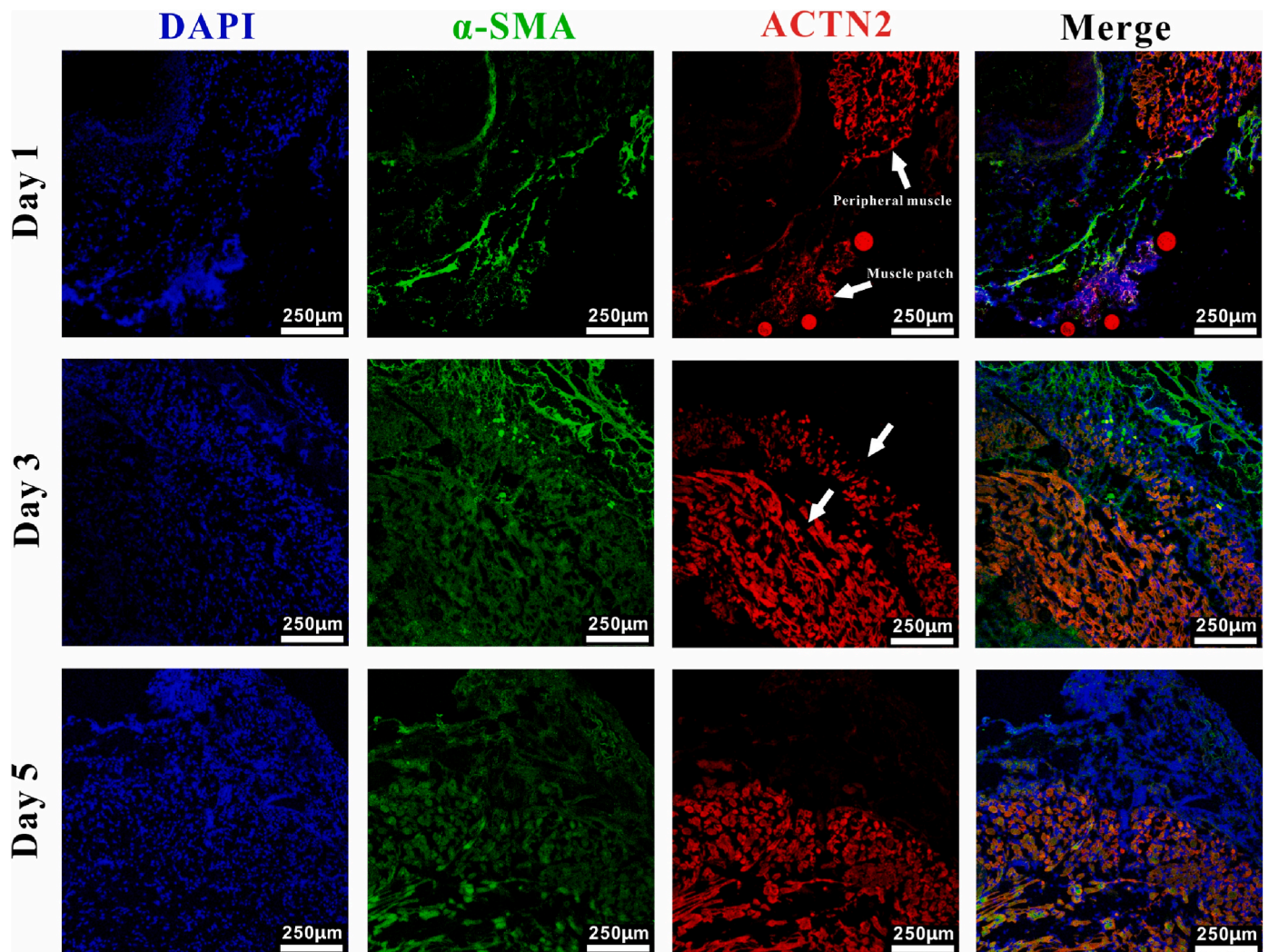
Fig. 9. Expressions of α-SMA and ACTN2 analyzed by IF on day 1, day 3 and day 5. The white arrows refer to ACTN2 expression at various locations.

muscle patch in the animal's body. On the first day post-operation, the engineered muscle patch exhibited significant Ki67 expression, with higher fluorescence intensity than the SMCs around the defect site (Fig. S8b, indicated by white arrow). This finding suggested that the *in vitro* constructed muscle demonstrated viability and robust proliferation capability during *in vivo* implantation. By day 3, the outer muscle layer initiated the repair process, with muscle cells migrating from the outer to inner regions, while the inner muscle repair still relied on the migration of peripheral muscle cells (Fig. 8a, Muscle patch, indicated by orange arrows). This observation suggests that the supportive muscle patch contributed its own cells to migrate to the defective muscle site, expediting muscle repair. By day 5, the defective muscle tissue was nearly completely repaired (Fig. 8b, Muscle patch).

The expression of α-SMA and ACTN2 in the regenerated muscle was assessed using IF technology during the repair process. The results indicated that both the muscle patch and the surrounding muscles maintained α-SMA expression throughout the wound repair process. ACTN2 is closely associated with the contraction function of smooth muscle, which helps assess the recovery of muscle contraction function [21]. At day 1, the expression level of ACTN2 in the engineered muscle was lower than that in the muscle tissue adjacent to the defect site (indicated by white arrows in Fig. 9). This finding aligns with the tension measurement results, where the contractility of the constructed muscle was not as strong as that of normal muscle tissue. Similar results were observed on the third day (indicated by white arrows in Fig. 9). The

expression of ACTN2 in the inner muscle, which relied on the migration of peripheral cells, was higher than that in the outer muscle, representing the grafted muscle patch. This is consistent with the idea that the repair of the outer muscle depends on cell migration from the engineered muscles. By day 5, the defective muscle had been repaired, and the expression of ACTN2 in the outer muscle was similar to that in the inner muscle, which was consistent with the results of histological analysis.

4. Discussion

In recent years, numerous tissue engineering strategies have been studied for the regeneration of smooth muscle in various tissues/organs, such as the intestines [22,23], blood vessels [24,25] and esophagus [26, 27] etc. In these studies, SMCs mainly relied on the scaffolds to achieve biological structure and cell functions. Comparatively, in this work, we first obtained a PEG scaffold with micro-channel patterns, and with the modification of Fe_3O_4 NPs, they aligned under the force of N/S magnetic fields. These scaffolds can not only promote the directional growth of SMCs but also induce a shift in SMC phenotype towards synthesis. As a result, we have achieved the successful engineering of muscle tissue patches in *in vitro* settings.

The primary focus of our *in vitro*-constructed muscle patch lies in assessing its functionality. Our engineered muscle patch could generate action potentials in response to *in vitro* stimulation, suggesting its
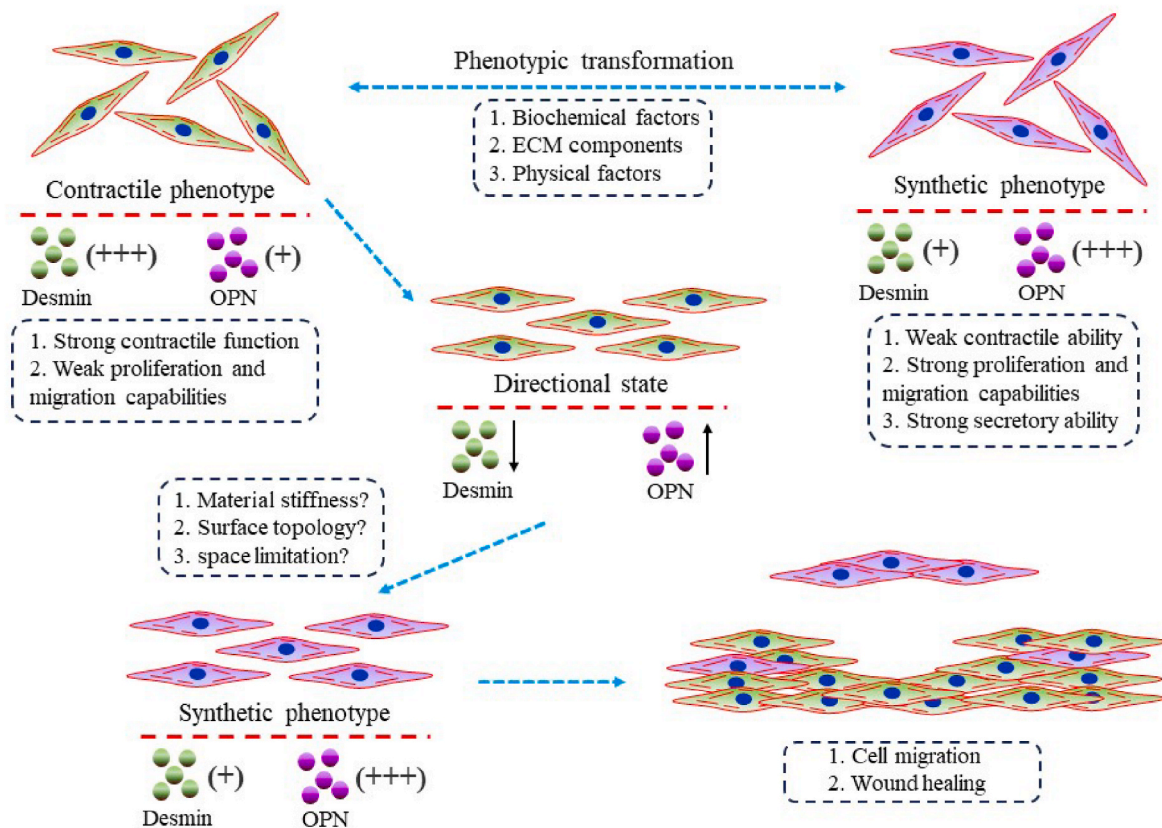
Fig. 10. Schematic representation of the mechanisms of the SMC phenotypic transformations and promotion of muscle healing.

potential for muscle contraction. Transcriptome sequencing was conducted using normal esophageal smooth muscle tissue as a control. The results of KEGG analysis indicated an enrichment of DEGs in the "Calcium signaling pathway." Additionally, GO analysis revealed that the down-regulated DEGs were associated with the biological process of "Muscle contract." Given that smooth muscle contraction relies on the activation of the "Calcium signaling pathway" and the interaction between myosin and actin [28,29], we conclude that the engineered muscle patch exhibits weaker contraction capabilities compared to normal muscle tissue. Moreover, GO analysis of up-regulated genes pointed toward the engineered muscle patches contributing to "wound healing." These observations can be attributed to the phenotype of SMCs cultured *in vitro*. Synthetic SMCs possess higher proliferative, migratory and secretory capacities but exhibit weaker contractile abilities than their contractile counterparts and can transition between these two phenotypes in response to changes in their extracellular environment, which may involve biochemical factors (e.g., TGF-β, activin A), extracellular matrix (ECM) components (e.g., proteoglycan heparin, Fibrillar collagen type I), and physical factors (e.g., tensile stress, shear stress) [18]. One study reported that SMCs on fiber substrates with high stiffness can switch to the synthetic phenotype [30]. In this study, material stiffness, surface topology and space limitation might have all affected the phenotypes of SMCs. While PEGM appears to encourage a shift toward a synthetic phenotype in SMCs, it is important to note that the cells maintain an intermediate state, as evidenced by the continued expression of α-SMA, a protein associated with the contractile phenotype, throughout the muscle patch generation process.

The results from animal experiments consistently confirm the viability and active participation of the engineered muscle patch in the repair of damaged muscle tissue when implanted *in vivo*, which plays a crucial role by contributing SMCs to fill the defective tissue and accelerate the regeneration of new muscle. Our findings suggest that muscle repair initiates with cell proliferation and migration from peripheral muscle cells to compensate for cell loss. The living muscle patch accelerates this process by providing a source of cells. The schematic representation in Fig. 10 summarizes the phenotypic transformations of SMCs and the muscle healing process.

Given the vital roles of muscle tissues in various organs and the prevalence of muscle-related diseases, which often lack effective clinical treatments, the muscle patch developed in this study holds great promise for enhancing the repair of muscle tissues in multiple organs and establishes a strong foundation with significant potential for future clinical applications. Numerous human organs and tissues, including the esophagus, stomach, intestine, blood vessels, trachea, iris, bile duct, bladder and ureter, contain smooth muscles and biological components. These smooth muscles are arranged in an organized manner, governing the movement and deformation of these organs and tissues. We anticipate that this engineered muscle could facilitate the regeneration and remodeling of all such muscle-containing organs, which will be the focus of our future research.

5. Conclusion

In summary, we have successfully constructed functional esophageal muscle tissue by utilizing magnetic Fe_3O_4 micro-/nano-stripes as alignment inducers on a microchannel-patterned scaffold, which could respond to *in vitro* stimuli and survive *in vivo*. Consequently, it facilitates the regeneration of esophageal muscle tissue and expedites muscle repair when implanted into the defect site in the rat's esophagus. Our analysis of DEGs indicates enrichment in processes such as "Cell migration", "Angiogenesis", "Wound healing" and "Extracellular matrix organization", providing evidence of the biological functions of this engineered muscle. We anticipate that this engineered muscle holds significant promise for future clinical applications, particularly in muscle-related diseases.

Authors' contributions

YL and YC: Data curation, administration, analysis and writing original draft. ZG, RN, PF, ZH, LS, XS, CG, JL and TD: Data curation and analysis. LY, HZ and YZ: Administration, funding acquisition, data verification and revise manuscript. All authors read and approved the final manuscript.

Declaration of competing interest

The authors declare that they have no known competing financial interests or personal relationships that could have appeared to influence the work reported in this paper.

Data availability

Data will be made available on request.

Funding and Acknowledgements

Appendix A. Supplementary data

Supplementary data to this article can be found online at https://doi.org/10.1016/j.mtbio.2023.100853.

References

[1] K.N. Bitar, Function of gastrointestinal smooth muscle: from signaling to contractile proteins, Am. J. Med. (2003) 15S–23S.

[2] J. Shi, Y. Yang, A. Cheng, G. Xu, F. He, Metabolism of vascular smooth muscle cells in vascular diseases, Am. J. Physiol. Heart Circ. Physiol. 319 (2020). H613-h31.

[3] L. Yin, N. Li, W. Jia, N. Wang, M. Liang, X. Yang, et al., Skeletal muscle atrophy: from mechanisms to treatments, Pharmacol. Res. 172 (2021), 105807.

[4] Y. Wang, Q. Liu, H. Quan, S.G. Kang, K. Huang, T. Tong, Nutraceuticals in the prevention and treatment of the muscle atrophy, Nutrients 13 (2021).

[5] M.S. Conceição, C. Ugrinowitsch, Exercise with blood flow restriction: an effective alternative for the non-pharmaceutical treatment for muscle wasting, Journal of Cachexia, Sarcopenia and Muscle 10 (2019) 257–262.

[6] M. Yeo, J.W. Yoon, G.T. Park, S.C. Shin, Y.C. Song, Y.I. Cheon, et al., Esophageal wound healing by aligned smooth muscle cell-laden nanofibrous patch, Materials Today Bio 19 (2023), 100564.

[7] L. Wang, Y. Wu, B. Guo, P.X. Ma, Nanofiber yarn/hydrogel Core-Shell scaffolds Mimicking native skeletal muscle tissue for guiding 3D myoblast alignment, elongation, and differentiation, ACS Nano 9 (2015) 9167–9179.

[8] S.H. Cha, H.J. Lee, W.G. Koh, Study of myoblast differentiation using multi-dimensional scaffolds consisting of nano and micropatterns, Biomater. Res. 21 (2017) 1.

[9] J. Stern-Straeter, F. Riedel, G. Bran, K. Hörmann, U.R. Goessler, Advances in skeletal muscle tissue engineering. *In Vivo* (Athens, Greece) 21 (2007) 435–444.

[10] T.H. Qazi, D.J. Mooney, M. Pumberger, S. Geissler, G.N. Duda, Biomaterials based strategies for skeletal muscle tissue engineering: existing technologies and future trends, Biomaterials 53 (2015) 502–521.

[11] M. Kobayashi, N.Y. Lei, Q. Wang, B.M. Wu, J.C. Dunn, Orthogonally oriented scaffolds with aligned fibers for engineering intestinal smooth muscle, Biomaterials 61 (2015) 75–84.

[12] J.S. Choi, Y. Piao, T.S. Seo, Circumferential alignment of vascular smooth muscle cells in a circular microfluidic channel, Biomaterials 35 (2014) 63–70.

[13] R. Hou, X. Wang, Q. Wei, P. Feng, X. Mou, Y. Zhu, et al., Biological properties of a bionic scaffold for esophageal tissue engineering research, Colloids and surfaces B, Biointerfaces 179 (2019) 208–217.

[14] C. Gong, L. Hou, Y. Zhu, J. Lv, Y. Liu, L. Luo, In vitro constitution of esophageal muscle tissue with endocyclic and exolongitudinal patterns, ACS Appl. Mater. Interfaces 5 (2013) 6549–6555.

[15] X. Wang, J. Jin, R. Hou, M. Zhou, X. Mou, K. Xu, et al., Differentiation of bMSCs on biocompatible, biodegradable, and Biomimetic scaffolds for Largely defected tissue repair, ACS Appl. Bio Mater. 3 (2020) 735–746.

[16] L. Jin, F. Cao, Y. Gao, C. Zhang, Z. Qian, J. Zhang, et al., Microenvironment-activated Nanozyme-Armed Bacteriophages efficiently Combat Bacterial infection, Advanced materials (Deerfield Beach, Fla) 35 (2023), e2301349.

[17] A. Huber, S.F. Badylak, Phenotypic changes in cultured smooth muscle cells: limitation or opportunity for tissue engineering of hollow organs? Journal of tissue engineering and regenerative medicine 6 (2012) 505–511.

[18] S.S. Rensen, P.A. Doevendans, G.J. van Eys, Regulation and characteristics of vascular smooth muscle cell phenotypic diversity, Neth. Heart J. : monthly journal of the Netherlands Society of Cardiology and the Netherlands Heart Foundation 15 (2007) 100–108.

[19] H. Hao, G. Gabbiani, M.L. Bochaton-Piallat, Arterial smooth muscle cell heterogeneity: implications for atherosclerosis and restenosis development, Arterioscler. Thromb. Vasc. Biol. 23 (2003) 1510–1520.

[20] T. Scholzen, J. Gerdes, The Ki-67 protein: from the known and the unknown, J. Cell. Physiol. 182 (2000) 311–322.

[21] W. Liu, Y. Zhao, J. Wu, Gene expression profile analysis of the progression of carotid atherosclerotic plaques, Mol. Med. Rep. 17 (2018) 5789–5795.

[22] Y. Chen, C. Guo, E. Manousiouthakis, X. Wang, D.M. Cairns, T.T. Roh, et al., Bi-Layered Tubular Microfiber scaffolds as functional Templates for engineering human intestinal smooth muscle tissue, Adv. Funct. Mater. 30 (2020).

[23] K.N. Bitar, S. Raghavan, E. Zakhem, Tissue engineering in the gut: developments in neuromusculature, Gastroenterology 146 (2014) 1614–1624.

[24] K. Qin, F. Wang, R.M.L. Simpson, X. Zheng, H. Wang, Y. Hu, et al., Hyaluronan promotes the regeneration of vascular smooth muscle with potent contractile function in rapidly biodegradable vascular grafts, Biomaterials 257 (2020), 120226.

[25] P. Wu, L. Wang, W. Li, Y. Zhang, Y. Wu, D. Zhi, et al., Construction of vascular graft with circumferentially oriented microchannels for improving artery regeneration, Biomaterials 242 (2020), 119922.

[26] P. Kuppan, S. Sethuraman, U.M. Krishnan, In vitro co-culture of epithelial cells and smooth muscle cells on aligned nanofibrous scaffolds, Mater. Sci. Eng., C 81 (2017) 191–205.

[27] L. Hou, C. Gong, Y. Zhu, In vitro construction and in vivo regeneration of esophageal bilamellar muscle tissue, J. Biomater. Appl. 30 (2016) 1373–1384.

[28] S. Salemi, J.A. Prange, V. Baumgartner, D. Mohr-Haralampieva, D. Eberli, Adult stem cell sources for skeletal and smooth muscle tissue engineering, Stem Cell Res. Ther. 13 (2022) 156.

[29] R.C. Webb, Smooth muscle contraction and relaxation, Adv. Physiol. Educ. 27 (2003) 201–206.

[30] B. Yi, Y. Shen, H. Tang, X. Wang, B. Li, Y. Zhang, Stiffness of aligned fibers regulates the phenotypic expression of vascular smooth muscle cells, ACS Appl. Mater. Interfaces 11 (2019) 6867–6880.